Microfluidic sieve-detector for rapid capture and detection of single molecules

Geunyong Kim[1,2], Molly L. Shen[1,2], Andy Ng[1,2] and David Juncker[1,2*]

1. Biomedical Engineering Department, McGill University, Montreal, QC, Canada
2. Victor Phillip Dahdaleh Institute of Genomic Medicine, McGill University, Montreal, QC, Canada

Abstract: Ultrasensitive, quantitative and simple tests for proteins and nucleic acids could empower analysis and disease diagnosis, but slowness of analyte capture and detection prevent it. We introduce the microfluidic sieve-detector (MSD) based on microfluidic Brownian affinity traps (BATs). A BAT is a micro-conduit coated with capture probes under commensurate flow such that an analyte flowed through binds a probe following Brownian motion-induced wall collision. Digital sandwich assays are completed by sequentially flowing the reagents, partitioning BATs, and revealing single 'trapped' analytes following enzymatic amplification. MSDs with arrays of half a million BATs sieved 200 microliters in just one minute, and quantified captured proteins (enzymes, IL-4, influenza nucleoprotein) and microRNA (miR-141) in four minutes, down to zeptomolar concentration. The MSD opens unprecedented analytical and diagnostic opportunities.

Main text: Rapid testing offers many advantages for diagnostics, but common approaches face trade-offs between sensitivity, time-to-result, simplicity and cost. Both protein and nucleic acid tests rely on binding between an analyte and a capture probe following their encounter upon diffusive, and sometimes convective, transport. Microfluidics has notably been used to shorten time-to-result by miniaturizing containers to speed-up diffusive mass transport (*1-3*); however, this comes at the expense of sensitivity because the inclusion of a statistically representative number of analytes requires ever larger sample volumes, while microchannels only accommodate microscopic volumes. A strategy to both accommodate larger volumes yet minimize the time and distance of diffusive transport between analyte and probes is to disperse the latter in solution, either directly or attached to microparticles (*4, 5*). Nucleic acid tests (*6-9*) disperse probes and use complementary base pairing recognition to initiate exponential amplification (*e.g.* polymerase chain reaction and isothermal amplification), which enables ultrasensitive detection, but at a comparatively long time-to-result of tens of minutes for low concentrations, while being limited by a small volumetric capacity of typically a few microliters only. Protein immunoassays have historically been less sensitive and conventional enzyme-linked immunosorbent assays (ELISAs) only use linear amplification (*10*) and are lengthy. Ultrasensitive immunoassays are possible by using digital detection of single molecules in samples within oil-partitioned 'dead-end' microwells or droplets (*11-15*). A breakthrough permitting robust, large volume processing was achieved by combining dispersed antibody-coated microparticles followed by partitioning them into microwells or droplets for digital detection (*16-20*); the microparticles capture and enrich analytes that are then sandwiched by detection antibody and enzyme for signal generation. However, the protocol remains lengthy (hours), the accuracy too variable for many diagnostic applications, and the instrumentation complex. Here we describe a microfluidic sieve-detector (MSD) that can sieve molecules very quickly using an isoporous membrane with each open-ended pore forming a Brownian affinity trap (BAT). Under commensurate sample flow, Brownian-motion induced wall collision leads to analyte capture within the BATs, which upon partitioning, turn into a digital detector array for quick counting and quantification of every 'trapped' analyte.

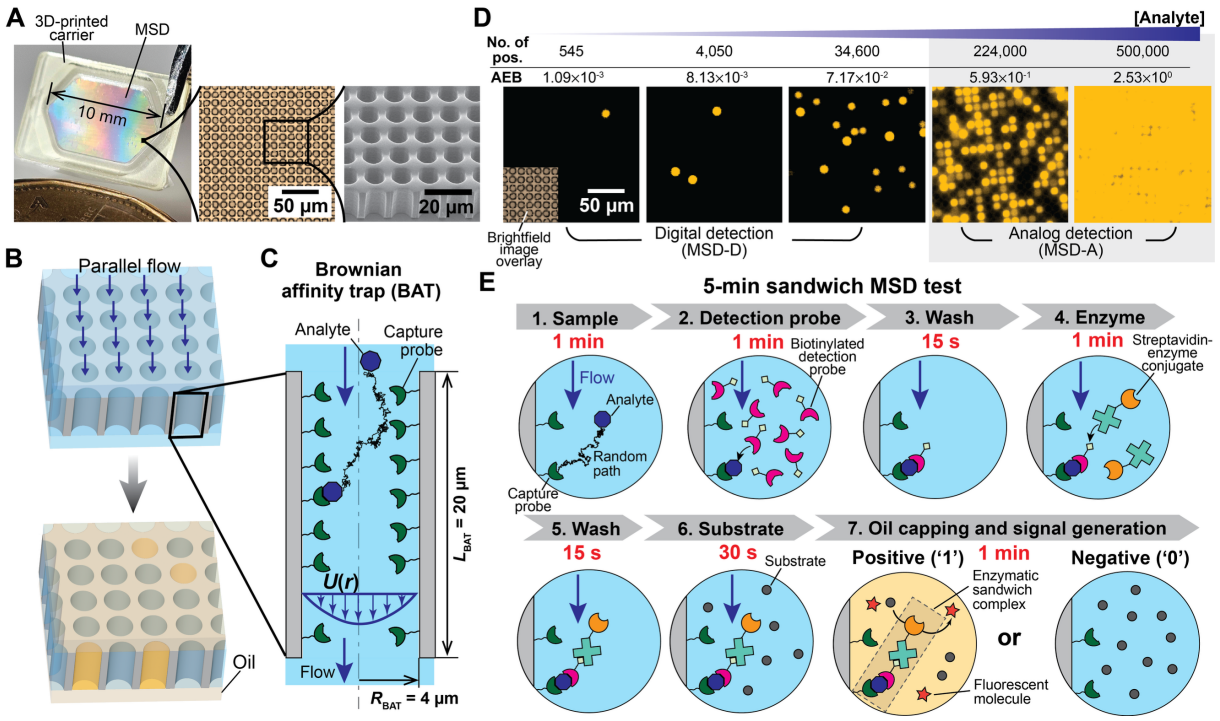

Fig. 1. Microfluidic sieve-detector (MSD) made from an array of Brownian affinity traps (BATs) captures and detects single analytes in 5 min. (**A**) MSD with 500,000 BATs bonded to a 3D-printed carrier with successive magnification. (**B**) MSD test concept. Sample, reagents and buffers are sequentially flowed through the MSD, BATs are partitioned by oil capping, and BATs that contain one or more captured analytes become fluorescent upon enzymatic amplification, digitally revealing single molecule binding. (**C**) Cross-section view of a 4 µm radius and 20 µm long BAT. A BAT is a microchannel coated with capture probe under commensurate flow promoting Brownian motion-induced wall collision of an analyte and affinity binding by the immobilized capture probe. The black trace reveals the path of a captured analyte. (**D**) Fluorescence image of positive BATs with positive counts and quantification by calculating the average number of enzymes per BAT (AEB). Quantification is achieved by digital counting (MSD-D) from ultralow to low concentrations, and by the average signal of the MSD (MSD-A) for higher concentrations, thereby extending the dynamic range of the test. (**E**) 5-min MSD test based on a sandwich immunoassay workflow. The sample with the analyte, biotinylated detection probe, enzyme conjugate, substrate and wash buffers are flowed sequentially for the indicated duration, followed by oil capping of the BATs, signal generation and quantification.

In this study, the MSD test has 800,000 pores cm^{-2} (40% open ratio; Fig. 1A) to permit rapid sieving of a sample at a high overall flow rate while meeting the commensurate, slow flow condition for a BAT. Each BAT is formed as a cylindrical, open-ended micropore with a radius R_{BAT} = 4 µm and a length L_{BAT} = 20 µm and single binding events are detected by enzymatic amplification following partitioning each BAT into a closed 1-pL compartment by oil capping (Fig.

1, B and C). Akin to other digital sandwich assays, a single enzyme rapidly generates easily detectable fluorescence in the microscopic BAT, thus permitting binary classification of BATs into positive ('1') and negative ('0'). As concentration increases, more BATs turn positive while the probability of more than one analyte per BAT also increases, which is predicted and compensated for by Poisson statistics and by calculating the average number of enzymes per BAT (AEB). For high percentage of positives (≳50%), AEB calculations become imprecise, but conversely analog readout becomes possible simply by measuring the average fluorescence signal of the MSD (see method for signal readout details). Hence MSDs operate with combined digital (MSD-D) and analog (MSD-A) detection, Fig. 1D (*17*). An MSD test is completed by flowing the sample, biotinylated detection probe, streptavidin-enzyme conjugate, and wash buffers through the MSD, then partitioning the BATs with oil and detecting analyte binding by enzymatic conversion of a soluble substrate in each BAT, all within only 5 min (Fig. 1E and see figs. S1 and S2 in supplementary section S1 for experimental setup and large-area MSD images with digital signals). Three critical features for MSD tests are (i) arrays of open-ended micropores (i.e. BATs) that are ~1,000 times larger than the sieved 'particles', facilitating clogging-free flow and affinity sieving, while minimizing the required pressure head, (ii) exclusive capture of analytes inside of the BATs, and not on the top and bottom surfaces between the BATs to preserve proportionality between number of molecules and positive counts, and (iii) leak-free capping with oil to partition BATs and enable digital readout.

Theoretical capture efficiency of the MSD and the BAT

A key metric of the MSD test is the analyte capture efficiency η of both the MSD and the BAT defined as the fraction of trapped to total analytes flowed through the MSD and BAT. We calculate η theoretically by ensemble (i) analytical and (ii) finite element method (FEM) calculations of binding reactions and by the (iii) stochastic Brownian-agent method (SBAM) we introduce. SBAM is a computational simulation of the Brownian motion of an analyte (the Brownian agent) as a random walk in the BAT under flow, while wall collision and affinity binding are simulated as stochastic events (*21-23*). SBAM visualizes single analytes, is intuitive and accounts for the stochasticity and stochastic variance that are ignored by ensemble models, while accurate η are obtained by Monte Carlo estimation upon repeated simulations. We presume geometrical ergodicity implying that the η of a single BAT calculated by SBAM is equivalent to the η of a

MSD, and concentration ergodicity implying that ensemble calculations of the reaction η of a BAT as the concentration change from inlet to outlet is equivalent to the capture η of single molecules flowing through a BAT. For all models, we consider that analytes enter the BAT pore with a length L_{BAT} and a radius R_{BAT}, at an average flow velocity $\bar{U}$ following a parabolic Poiseuille flow profile and are subject to Brownian motion according to the diffusion coefficient D [m^2 s^{-1}], see Fig. 1C.

For the ensemble models, we consider the on-rate k_{on} [m^3 mol^{-1} s^{-1}] under first-order Langmuir kinetics, the surface density of the immobilized capture probe Γ [mol m^{-2}], and the surface-to-volume ratio $2/R_{BAT}$. We define $\kappa_{on} = 2k_{on}\Gamma/R_{BAT}$ [s^{-1}] as the effective on-rate and $\tau_{res} = L_{BAT}/\bar{U}$ [s] as the average residence time of the sample. In this study, we operate under conditions of large κ_{on} (~10^{-1}–10^2 s^{-1}), low density of bound analyte, and short timescales with low off-rates k_{off} (~10^{-6} s^{-1}), so that dissociation can be neglected in the analysis. The Péclet (Pe) and Graetz (Gz) numbers quantify the ratio of convective to diffusive transport and are > 1 for all experiments, indicating convection-dominated transport. Damköhler numbers (Da) express the ratio of the reaction to mass transport rates and we consider the first Damköhler number, $\mathrm{Da_I} = \kappa_{on}\tau_{res}$ representing the ratio of reaction rate to convective mass transport and a surface Damköhler number, $\mathrm{Da_s} = k_{on}\Gamma/k_c$ with k_c [m s^{-1}] being the mass transfer coefficient used in thin film theory, and which is the ratio of reaction rate to the total mass transport to the surface including both convection and diffusion (supplementary section S2 and fig. S3) (*1, 24, 25*). We calculate the ensemble reaction efficiency η of a BAT following classical derivations (*25-27*) and find (supplementary section S3 and fig. S4 for the detailed derivation):

$$\eta = 1 - e^{\frac{-\mathrm{Da_I}}{1+\mathrm{Da_s}}} \tag{1}$$

For all experiments in this study, $\mathrm{Da_s} < 1$, hence we obtain:

$$\eta = 1 - e^{-\mathrm{Da_I}} \tag{2}$$

Hence, η is adjustable by varying κ_{on} (*e.g.* via the surface density of capture probes) and τ_{res} via $\bar{U}$. The FEM ensemble calculations directly solve the coupled convection-diffusion-reaction equations without simplifying assumptions and provide spatially resolved concentration fields, from which η is obtained as the ratio of the outlet to inlet average concentration, Fig. 2, A and B. SBAM analysis is described in detail in supplementary section S4 including the computational algorithm in fig. S5. Example traces visualizing random-walk analyte trajectories under different

flow conditions and varying surface affinity, are shown as slow-motion, time-stamped animations in movies S1–S3, and as traces superposed with FEM ensemble models of concentration in Fig. 2, A and B.

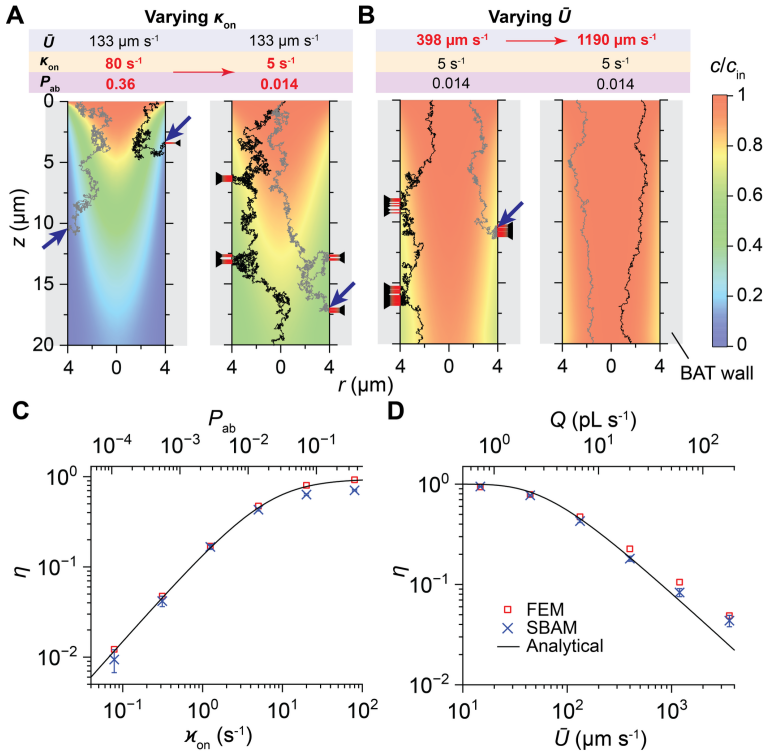

Fig. 2. Stochastic Brownian-agent method (SBAM) traces and analytical, SBAM and FEM calculations of BAT capture efficiency η for different conditions. (**A**) SBAM example traces overlaid on FEM simulation for a model 100 kDa globular protein analyte with a diffusion coefficient D = 80 μm^2 s^{-1} with varying effective on-rate κ_{on} and affinity binding probability P_{ab} at a fixed average flow speed, $\bar{U}$ = 133 μm s^{-1}, and with (**B**) varying $\bar{U}$ at fixed κ_{on} = 5 s^{-1} and P_{ab} = 0.014. Arrows record analyte binding while red bars with a black arrow tail indicate wall collision without binding. The color bar indicates the ratio, c/c_{in}, where c is the local analyte concentration and c_{in} is the inlet concentration. (**C**) η as a function of κ_{on} at $\bar{U}$ = 133 μm s^{-1} and (**D**) of $\bar{U}$ at κ_{on} = 5 s^{-1}. SBAM error bars represent the 95% confidence interval of SBAM with N = 5,000 and increase for low η due to stochastic noise.

To calibrate SBAM, we introduce the affinity binding probability upon wall collision (P_{ab}) as a free parameter. Benchmarking against η obtained from the FEM calculations, calibration was performed for the model system with a 100 kDa globular protein analyte with D = 80 μm^2 s^{-1} flowing at $\bar{U}$ = 10 μm s^{-1}. P_{ab} was determined and found to be proportional to κ_{on} (supplementary

section S4 and fig. S6) for a wide range of κ_{on}, and constant relative to τ_{res} (and $\bar{U}$) across a broad range, Fig. 2, C and D. A lower κ_{on} (and lower P_{ab}) result in a higher number of non-binding collisions, and a lower τ_{res} in fewer wall collisions, both contributing to lower η. The calibrated SBAM was consistent with both FEM and analytical calculations while capturing stochastic variances of single-analyte binding in BATs.

MSD membrane manufacturing and functionalization

MSDs were made by molding and photopolymerization of a perfluoropolymer forming an isoporous membrane almost identical to the one used for size-exclusion-based filtration of circulating tumor cells (*28, 29*), but used here for Brownian affinity trapping of molecular analytes inside of the pores. A crucial prerequisite for MSD assays is two-sided hydrophobicity of the membrane to both prevent unwanted binding of the analytes on the 'top surface', outside of the BAT, which could confound assay results, and to form a water-tight seal upon capping with fluorinated oil and partition each BAT for digital assay readout. We developed float-flip-float process to exclusively functionalize the inside of BATs with capture probes and preserve hydrophobicity on the top and bottom surfaces of MSDs as described in supplementary section S5 and shown in fig. S7.

Experimental efficiency of the MSD and of the BAT

We systematically evaluated MSD and BAT sieving η experimentally with an array of 500,000 BATs. The captured analytes were directly detected via a one-step MSD test, Fig. 3A; see supplementary section S1 and fig. S1 for experimental details. Briefly, MSDs were functionalized with biotin as a capture probe, and streptavidin-β-galactosidase conjugate (SβG) was used as a combined "analyte-detection probe-enzyme". The direct detection of the captured analytes eliminates confounding factors arising from downstream steps such as detection probe and enzyme incubations that contribute to false positives and negatives. We independently established κ_{on} = 7.44 s^{-1} and P_{ab} = 0.035 with high density functionalization (for details on κ_{on}, see figs. S8 and S9, and table S1 in supplementary section S6).

In typical experiments, 200-μL-samples were sieved at a flow velocity of $\bar{U}$ = 133 μm s^{-1} for 1 min and the captured molecules were detected following sequential 1-min steps of washing and flowing of resorufin-β-D-galactopyranoside (RGP), followed by oil capping and enzymatic

conversion of RGP into fluorescent resorufin. We evaluated the number of captured molecules as a function of the volume over 2 OM and observed the expected proportionality, Fig. 3B. The MSD and BAT efficiency η was quantified by calculating the ratio of captured to total number of molecules flowed under varying conditions, and compared to theory. We varied flow velocity (and corresponding flow rate) and κ_{on} (and corresponding P_{ab}) over at least 2 OM each. κ_{on} was modulated by varying the surface density of biotin serving as the capture probe by ratiometric incorporation of spacer molecules and via different capture probe types. We compared experimental results with analytical, FEM and SBAM predictions, and found strong concordance in all cases, Fig. 3, C and D, thus mutually validating and reinforcing theory (notably SBAM analysis) and experimental findings. The data showcase rapid, predictable and tunable analyte capture by microfluidic sieving of 200 μL in just 2 s with $\bar{U}$ = 3,580 μm s^{-1} for η ~ 2% (characteristic convection time 10^{-3} s << reaction time ~10^{-1} s < characteristic diffusion time ~ 1 s), and in 1 min with $\bar{U}$ = 133 μm s^{-1} for η ~ 50% (with similar characteristic convection and reaction times of ~10^{-1} s), for diverse capture probes including biotin, antibodies and nucleic acids, and with linearly increasing numbers with volume.

Next we evaluated how a high η ~ 50% could benefit assay performance for the one-step test by establishing a standard binding curve for varying concentrations of SβG. We used dynamic thresholding to distinguish positive and negative BATs that proved robust with a coefficient of variation (CV) of 9%, but with residual false-positives (AEB ~10^{-4}) at zero concentration, Fig. 3E. Both the stochastic analyte capture with its standard error (that can be evaluated using the SBAM simulation), and stochastic sampling with Poisson noise, each leading to increased fluctuations scaling with the square root, contribute to CV and become significant for low analyte numbers. The overall noise fluctuated from 40% below the limit of detection (LOD) to 11% in the linear range, which we consider to be good for a manual test. The readout accuracy drops for AEB > 0.5 because increasing number of BATs will have more than one analyte, and for test results above this threshold average fluorescence signals are quantified by MSD-A readout. With the combined MSD-D and MSD-A, we obtained an LOD of 35.9 zM and a linear dynamic range of ~7 OM for a 4-min-test, which is remarkable.

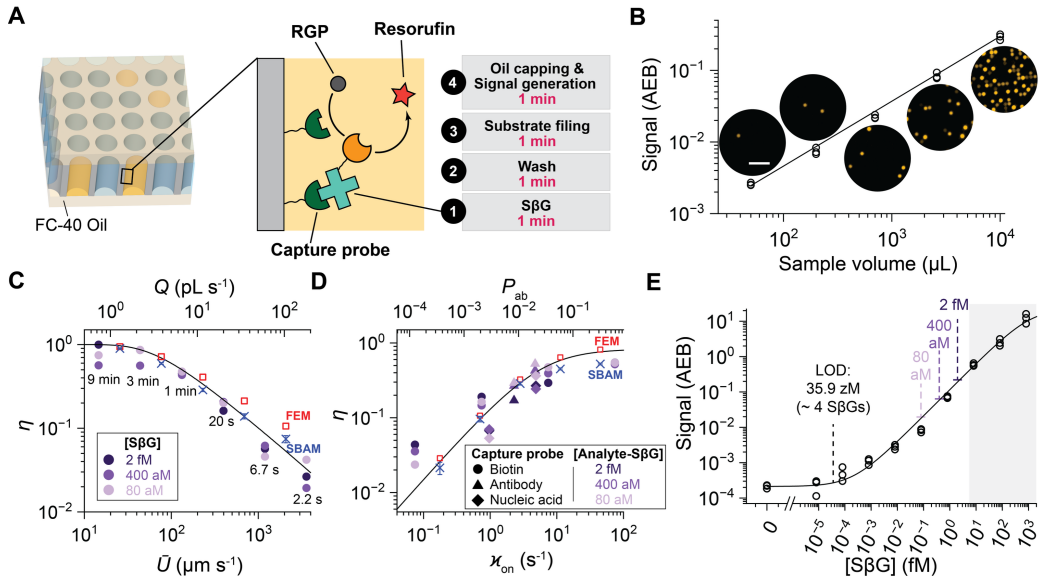

Fig. 3. Experimental one-step MSD test sieving efficiency η is concordant with theory. MSD tests were conducted using a 200 μL solution containing streptavidin-β-galactosidase (SβG, MW = 530 kDa and D = 45.9 μm^2 s^{-1}) flowed through an array of 500,000 BATs in 1 min with $\bar{U}$ = 133 μm s^{-1} and with κ_{on} = 7.44 s^{-1}, unless indicated otherwise. (**A**) Workflow of one-step MSD test with SβG "analyte-detection probe-enzyme". (**B**) The number of captured analytes (i.e., AEB) as function of sample volume follows a linear relationship with a slope of 0.91 and R^2 = 0.99. Insets are illustrative MSD images. Scale bar = 50 μm. Experimental sieving efficiency η as function of (**C**) flow speed $\bar{U}$ (and corresponding flow rate Q and incubation times) and of (**D**) κ_{on} (and corresponding P_{ab}) for different capture probes (biotin, antibody, nucleic acid each with its corresponding analyte-SβG system) and varying surface density for each probe. η was measured for analyte concentration of 2 fM, 400 aM and 80 aM, and found to be invariable as expected. Line is analytical model, squares are FEM and '×' is SBAM. (**E**) MSD standard binding curve for this 4-min test (see A). The white and grayed areas of the curve correspond to MSD-D and MSD-A, respectively. The limit of detection (LOD) was defined as the concentration yielding an AEB equal to the mean of the zero-concentration sample plus three standard deviations, accounting for both experimental and Poisson noise.

MSD test with sandwich binding for quantification of proteins and nucleic acids

We extended MSD tests to sandwich assays for proteins as well as nucleic acids with a time-to-result of 5 min accounting for capture and digital detection of molecules (See Fig. 1E and fig. S1 in supplementary section S1). Similar to a conventional ELISA, the sandwich MSD test is based on sequentially introducing the sample containing the analyte, biotinylated detection probe

and the streptavidin-enzyme conjugate (*i.e.* SβG in our case), leading to an enzymatic sandwich complex, which then produces fluorescent resorufin from RGP (Fig. 4A). The sandwich format introduces additional sources of noise, and most significantly the non-specific binding of either the detection probe or of SβG each contribute to false positive BATs. False positives quickly degrade assay sensitivity and performance, and should be kept low (*18*). We thus systematically optimized blocking, reagent concentration, flow time, flow speed to reach a background signal for negative controls of ~10^{-3} AEB, *i.e.* ~500 positive BATs for an MSD with 500,000 BATs. Standard curves for IL-4 and influenza A nucleoprotein were generated with the 5-min MSD test and with a classical 4-h ELISA in microplates, Fig. 4, B and C. The LODs of the ELISA were 118 fM (1.77 pg ml^{-1}) and 918 fM (52.1 pg ml^{-1}), respectively, and of the MSD 325 aM (4.88 fg ml^{-1}) and 2.00 fM (113 fg ml^{-1}), respectively. The dynamic ranges were ~ 2 OM for the ELISA, and 7 OM for the combined MSD-D and MSD-A. The MSD was thus 50 times faster and ~350 times more sensitive, and dynamic range was extended not only at the low, but also at the high concentration range by 2-3 OM *vs* ELISA. The LOD and CVs of the MSD test are similar or better compared to other ultrasensitive assays, but with a time-to-result of only 5 min *vs* 2–4 h (*16-20*).

We evaluated whether MSD tests could be used for nucleic acid detection and compared it to polymerase chain reaction (PCR), which serves as a gold standard. We selected miR-141 as the target analyte because it is small and compatible with sandwich-based detection needed for SβG binding and enzymatic amplification (Fig. 4D). The LOD of the MSD tests was 7.05 fM for a 200 μL sample, again with a 5 min time-to-result (Fig. 4E) which we found to rival the LOD of reverse-transcription quantitative PCR (RT-qPCR) that was 1.93 fM at the background cycle threshold (Ct) of 35. However, PCR lasted for 2h and operated from < 1 μL of effective sample volume (fig. S10). Droplet digital PCR (ddPCR) was evaluated but did not outperform the MSD test; inefficient reverse transcription (RT) and numerous false-positive droplets caused by carryover of the RT primer limited sensitivity, failing detection of miR-141 even at 240 fM (data not shown). The MSD tests illustrates that linear enzymatic signal amplification in a microscopic volume (1 pL) with a high turnover rate (~10^3 s^{-1} for βG) (*30*) can detect molecules in < 1 min, thus outperforming the exponential amplification of PCR by thermocycling. PCR is further limited to ≲1 μL and a separate pre-concentration is required to increase sensitivity, while MSD sensitivity can be improved by sieving larger volume, here with up to 5 mL for 25 min sieving at the same flow rate and an improved LOD of 206 aM (Fig. 4F). The MSD test compares favorably to PCR with its

simpler protocol and instrumentation, shorter time-to-result, and improved LOD with larger volumes.

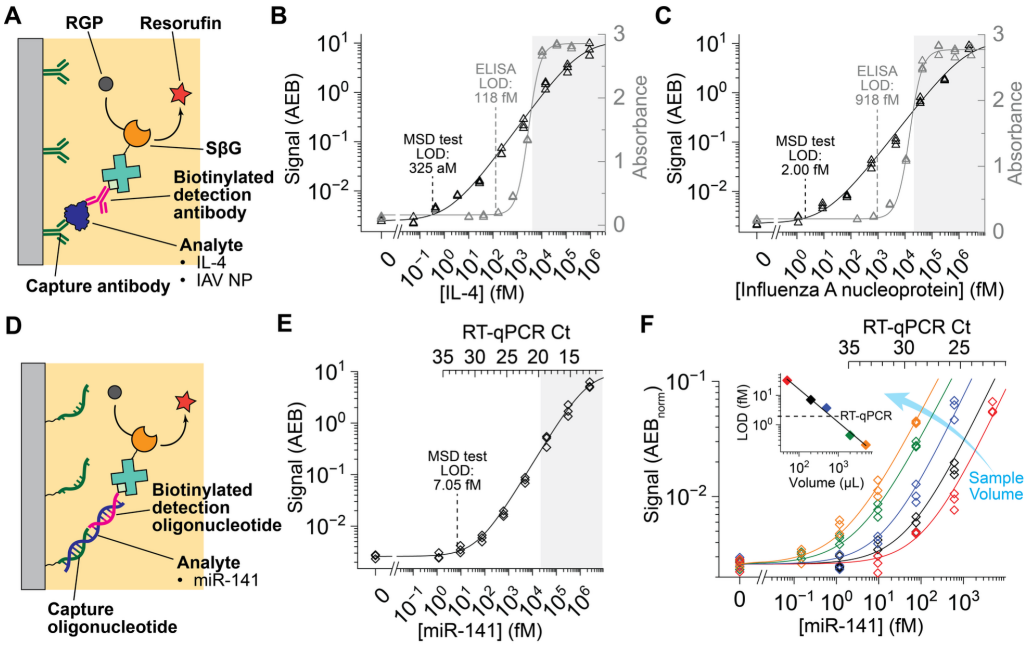

Fig. 4. Sandwich MSD test for detection of proteins and nucleic acids. (**A**) Sandwich complex for protein detection and standard curves of 5-min MSD test (**B**) for IL-4 and (**C**) for influenza A virus nucleoprotein. The standard curves from MSD test and the benchmark microplate ELISA are shown in black and gray, respectively. Grayed area is MSD-A detection. The coefficients of variation (CVs) for IL-4 and influenza A nucleoprotein are 14 and 12 %, respectively. (**D**) Sandwich complex for nucleic acid detections. (**E**) Standard curve of 5-min MSD test for miR-141. The CV is 17%. Grayed area corresponds to MSD-A detection. (**F**) Standard curves for volumes of 50 μL (red), 200 μL (black, reference), 500 μL (blue), 2 mL (green) and 5 mL (orange). All samples were flowed at 200 μL min^{-1} followed by the 4 min detection, resulting in total assay times of 4.25, 5, 6.5, 14 and 29 min, respectively. The inset shows LODs for varying sample volumes and corresponding LOD for RT-qPCR as dashed line. All LODs were defined as the concentrations yielding an AEB three standard deviations above the mean AEB of the zero-concentration sample.

Influenza A virus detection from nasopharyngeal swab samples

To evaluate the potential of the MSD for clinical translation, we tested 15 influenza A-positive and 15 negative samples obtained via nasopharyngeal swabbing and diagnosed using RT-

qPCR (See table S2 for demographics), and compared it to a commercial rapid test. Influenza A nucleoprotein was released by adding lysis buffer, waiting for 5 min, and measuring the sample using both the 15-min rapid test and the 5-min MSD test (Fig. 5A). The rapid test detected 6 out of 15 positives (fig. S11), yielding 40% sensitivity (95% CI, 20–64%), and 100% specificity (95% CI, 80–100%). The MSD test detected all positives including those missed by the rapid test, with one false positive (Fig. 5B), yielding 100% sensitivity (95% CI, 80–100%) and 93% specificity (95% CI, 70–99%; see fig. S12 for confusion matrices of both tests). Receiver operating characteristic (ROC) curve yielded an area under the curve (AUC) of 0.98 and 0.83 for the MSD and rapid test (Fig. 5C), respectively. In this small cohort, the MSD test expectedly outperformed rapid tests while matching PCR sensitivity. Larger cohorts and further investigation will be needed to accurately benchmark MSD tests. These results illustrate the potential of the MSD as a rapid, ultrasensitive diagnostic test. The intrinsic sensitivity of the MSD suggests a potential for improved diagnostic sensitivity compared to PCR when considering that there are ~2,000 nucleoproteins for 1 genetic copy per influenza A virus.

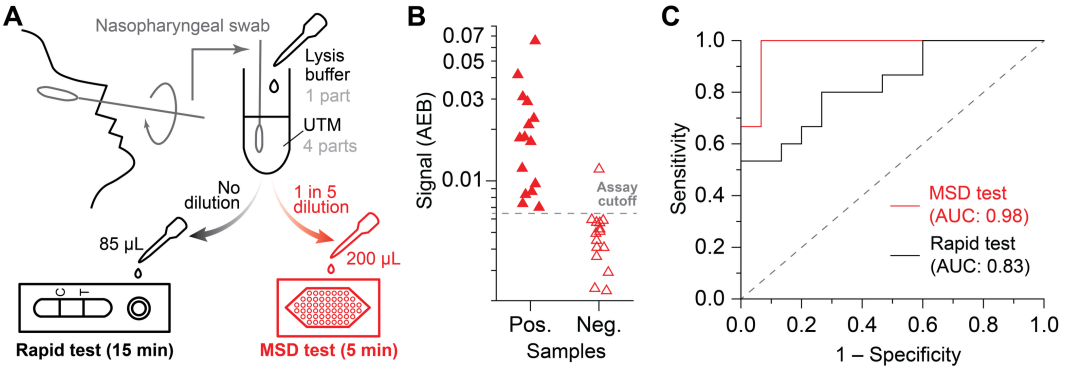

Fig. 5. Influenza A detection from nasopharyngeal swab samples. (**A**) Assay workflow. Nasopharyngeal swab samples in universal transport medium (UTM) were lysed to release influenza A virus nucleoprotein. The samples were then tested by both a 15-min rapid test without dilution and the 5-min MSD test after a 5-fold dilution. (**B**) MSD test results of 15 positive and 15 negative samples. (**C**) Receiver operating characteristic (ROC) curves for rapid test and MSD test. Areas under the curve (AUCs) for the rapid test and MSD test were evaluated as 0.83 and 0.98, respectively.

Conclusion

We introduced the MSD based on a large array of BATs for rapid, efficient capture of analytes, and ultrasensitive, *in situ* digital (and analog) detection in 5 minutes. The capture

efficiency η is predictable based on flow rates and effective on-rates (κ_{on}), and was confirmed by the proposed SBAM, ensemble analytical and FEM calculation, and experiments. ~50% of molecules in a 200-μL-sample could be captured in just 1 min sieving with 500,000 BATs at $Da_I \sim 1$ and $Da_s < 1$. Conventional sieves rely on size-exclusion and depend on pores being smaller than the targets, but the diameter of BATs is over 1,000 times larger than target analytes and minimizes both clogging and the sieving pressure head. The MSD showcases the hitherto untapped potential of vertical flow-through in sensor design that enables rapid capture, and together with partitioning and fast enzymatic signal amplification, make for an overall fast and ultrasensitive test, and endow it with a broad dynamic range of seven orders of magnitude and a low CV suitable for quantification. The MSD transcends traditional trade-offs of speed *vs* sensitivity, all while being simple, adaptable (*e.g.* proteins and nucleic acids were measured), and highly specific thanks to the sandwich assay set-up. The MSD is a thin, isoporous polymer membrane and is predisposed for integration and for automation thanks to a flow through protocol. The MSD may be further improved and tuned via BAT size and numbers and via sample volume from microliters to milliliters, and used for various analytes and samples. Existing and new applications, and unmet needs in various fields, stand to gain from rapid, ultrasensitive analytical and diagnostic MSD tests.

References and Notes

1. T. M. Squires, R. J. Messinger, S. R. Manalis, Making it stick: convection, reaction and diffusion in surface-based biosensors. *Nat. Biotechnol.* **26**, 417-426 (2008).
2. S. Cesaro-Tadic *et al.*, High-sensitivity miniaturized immunoassays for tumor necrosis factor α using microfluidic systems. *Lab Chip* **4**, 563-569 (2004).
3. M. Yafia *et al.*, Microfluidic chain reaction of structurally programmed capillary flow events. *Nature* **605**, 464-469 (2022).
4. M. F. Elshal, J. P. McCoy, Multiplex bead array assays: Performance evaluation and comparison of sensitivity to ELISA. *Methods* **38**, 317-323 (2006).
5. M. Dagher *et al.*, nELISA: A high-throughput, high-plex platform enables quantitative profiling of the inflammatory secretome. *bioRxiv*, 2023.04.17.535914 (2025); (in-press, *Nat. Methods*)
6. K. B. Mullis, F. A. Faloona, in *Methods Enzymol.* (Academic Press, 1987), vol. 155, pp. 335-350.
7. B. J. Hindson *et al.*, High-Throughput Droplet Digital PCR System for Absolute Quantitation of DNA Copy Number. *Anal. Chem.* **83**, 8604-8610 (2011).
8. Y. Zhao, F. Chen, Q. Li, L. Wang, C. Fan, Isothermal Amplification of Nucleic Acids. *Chem. Rev.* **115**, 12491-12545 (2015).
9. F. Shen *et al.*, Digital Isothermal Quantification of Nucleic Acids via Simultaneous Chemical Initiation of Recombinase Polymerase Amplification Reactions on SlipChip. *Anal. Chem.* **83**, 3533-3540 (2011).
10. E. Engvall, P. Perlmann, Enzyme-linked immunosorbent assay (ELISA) quantitative assay of immunoglobulin G. *Immunochemistry* **8**, 871-874 (1971).
11. Y. Rondelez *et al.*, Microfabricated arrays of femtoliter chambers allow single molecule enzymology. *Nat. Biotechnol.* **23**, 361-365 (2005).
12. S. Ge, W. Liu, T. Schlappi, R. F. Ismagilov, Digital, ultrasensitive, end-point protein measurements with large dynamic range via brownian trapping with drift. *J. Am. Chem. Soc.* **136**, 14662-14665 (2014).
13. S. Honda, Y. Minagawa, H. Noji, K. V. Tabata, Multidimensional Digital Bioassay Platform Based on an Air-Sealed Femtoliter Reactor Array Device. *Anal. Chem.* **93**, 5494-5502 (2021).
14. S. A. Byrnes *et al.*, Wash-Free, Digital Immunoassay in Polydisperse Droplets. *Anal. Chem.* **92**, 3535-3543 (2020).
15. B. H. Han, M. Park, S. Chung, J. Y. Kang, Evaporation-driven digital ELISA with micro-droplet arrays for ultrafast detection of low-abundance proteins. *Biosens. Bioelectron.* **292**, 118076 (2026).
16. D. M. Rissin *et al.*, Single-molecule enzyme-linked immunosorbent assay detects serum proteins at subfemtomolar concentrations. *Nat. Biotechnol.* **28**, 595-599 (2010).
17. D. M. Rissin *et al.*, Simultaneous Detection of Single Molecules and Singulated Ensembles of Molecules Enables Immunoassays with Broad Dynamic Range. *Anal. Chem.* **83**, 2279-2285 (2011).
18. C. W. Kan *et al.*, Digital enzyme-linked immunosorbent assays with sub-attomolar detection limits based on low numbers of capture beads combined with high efficiency bead analysis. *Lab Chip* **20**, 2122-2135 (2020).
19. V. Yelleswarapu *et al.*, Mobile platform for rapid sub–picogram-per-milliliter, multiplexed, digital droplet detection of proteins. *Proc. Natl. Acad. Sci. U.S.A.* **116**, 4489-4495 (2019).

20. L. Cohen *et al.*, Single Molecule Protein Detection with Attomolar Sensitivity Using Droplet Digital Enzyme-Linked Immunosorbent Assay. *ACS Nano* **14**, 9491-9501 (2020).
21. H. Risken, in *The Fokker-Planck equation: methods of solution and applications*. (Springer, 1989).
22. G. Fullstone, J. Wood, M. Holcombe, G. Battaglia, Modelling the Transport of Nanoparticles under Blood Flow using an Agent-based Approach. *Sci. Rep.* **5**, 10649 (2015).
23. M. Tracy, M. Cerdá, K. M. Keyes, Agent-based modeling in public health: current applications and future directions. *Annu. Rev. Public Health* **39**, 77-94 (2018).
24. R. B. Bird, W. Stewart, E. N. Lightfoot, *Transport Phenomena second edition*. (John Wiley & Sons, 2002).
25. T. Gervais, K. F. Jensen, Mass transport and surface reactions in microfluidic systems. *Chem. Eng. Sci.* **61**, 1102-1121 (2006).
26. G. M. Brown, Heat or mass transfer in a fluid in laminar flow in a circular or flat conduit. *AIChE Journal* **6**, 179-183 (1960).
27. W. M. Deen, *Analysis of Transport Phenomena*. (OUP USA, 1998).
28. J. A. Hernández-Castro, K. Li, A. Meunier, D. Juncker, T. Veres, Fabrication of large-area polymer microfilter membranes and their application for particle and cell enrichment. *Lab Chip* **17**, 1960-1969 (2017).
29. A. Meunier *et al.*, Gravity-based microfiltration reveals unexpected prevalence of circulating tumor cell clusters in ovarian and colorectal cancer. *Commun. Med.* **5**, 33 (2025).
30. D. M. Rissin, H. H. Gorris, D. R. Walt, Distinct and Long-Lived Activity States of Single Enzyme Molecules. *J. Am. Chem. Soc.* **130**, 5349-5353 (2008).

Ethics statement: Nasopharyngeal swab samples were obtained from American Blood Services DBA, Los Osos, CA, USA. According to the supplier's certification, all samples were collected under an appropriate institutional review board (IRB) protocol (IRB approval ID: 45469786).

Acknowledgements: We gratefully acknowledge M. Tabrizian and J.V.L. Nguyen for access to their SPR system and assistance, A. Kamen, J. Fulber and X. Xu for access to their ddPCR system and assistance, D. Liu at the Facility for Electron Microscopy Research of McGill University for help in microscope operation and data collection, C. Yansouni and J. Papenburg for discussions and advice, T. Gervais for proof-reading, Tri-iso and Ingevity for providing CAPA 3050 samples and Allnex for providing Ebecryl® 3708 and Tripropylene glycol diacrylate (TPGDA) samples.

Funding: This research was supported by The Natural Sciences and Engineering Research Council of Canada (NSERC) Discovery Grant RGPIN-2022-05171, Canada Research Chair in Bioengineering CRC-232159, and McGill University MI4 Emergency COVID-19 Research Funding and Pathy Seed Fund Grant. G.K. acknowledges an FRQNT doctoral research scholarship and a McGill BME recruitment award. M.L.S acknowledges a Vanier Canada Graduate Scholarship and a McGill BME recruitment award.

Author contributions:

Conceptualization: G.K., A.N., D.J.

Methodology: G.K., A.N., D.J.

Investigation: G.K., M.L.S.

Visualization: G.K., M.L.S.

Funding acquisition: A.N., D.J.

Supervision: D.J.

Writing – original draft: G.K., A.N., D.J.

Writing – review & editing: G.K., M.L.S., A.N., D.J.

Competing interests: G.K. and D.J. are inventors on a report of invention submitted to McGill University. All other authors declare no competing interests.

Data and materials availability: MATLAB codes for MSD image processing are available at https://github.com/junckerlab/MSD-readout. Data not presented in the article or supplementary material will be available upon request.